SPLASH, VORTICES AND TURBULENT SHEARS IN PARTIAL DAM-BREAK FLOWS – SPLASH MODEL OF WAVE-BREAKING AND OVERTOPPING –

Yasunori Watanabe[1], Shunichi Sato[2], Yasuo Niida[3], Ichiro Kimura[4], Hiroshi Yokota[5], Haruhi Oyaizu[6], Yuki Oshima[7] and Ayumi Saruwatari[8]

Three-dimensional evolution of local fluid flows and surface shapes under partial collapse of a water column is characterized during computational experiments using three-dimensional large eddy simulation in this paper. The free-surface behaviors highly depend on the collapse level and ambient water layer depth via mechanical interactions between the surface and vortices. It has been found major three modes of the splashing responses of the free-surfaces and vortex structures; (i) forward projection of secondary jets, which organizes a typical rib-like vortex structure stretched underneath the jets, (ii) backward jet projection with an inverse form of the rib structure, and (iii) blob-like waves induced by an array of the horizontal roller vortices. These findings provide new perspectives to understand wave breaking behaviors as well as practical assessments for the fluid responses in the splashing area for sea wall overflow and overtopping.

Keywords: wave breaking, overtopping, splash, vortex, LES

INTRODUCTION

A variety of surface forms of wave faces, jets and bores, depending on incident wave conditions, water depth and bottom slope, are observed after wave breaking. Although an initial stage of wave breaking is characterized by a breaker types or surf similarity parameter because of gravity-dominated phenomenon, the following dynamics is described by a combination of various mechanical effects including turbulence, vortices, shear and surface tension. The physical mechanisms to describe evolution of the local surface deformation and velocity have yet been well understood.

While the overturning waves initially produce a prominent two-dimensional roller vortex, three-dimensional vortex structures are often observed for being organized during a splash-up process. Nadaoka et al. (1989) found three-dimensional turbulent structures involving vortex pairs extending behind the breaking wave face in the direction of obliquely downward, a so-called obliquely descending eddy (ODE) (see Fig. 1). Watanabe (2005) interpreted the mechanism to change orientation of the initial spanwise vorticity on a two-dimensional roller vortex into obliquely downward to produce ODE via shear instability manifested at stagnation point flow at wave plunging locations. The resulting counter-rotating vortices stretched beneath the surface in the direction of wave propagation deform the free-surface, owing to surface entrainment, to configure a scarified surface shape (Sarpkaya and Suthon 1991). Saruwatari et al. (2009) interpreted that the development of the vorticity-induced scars on the secondary jets results in a formation of finger jets. Kubo and Sunamura (2001) experimentally found another type of vertical flows resulted from backward collapse of wave surfaces owing to horizontal counter-rotating vortices (see Fig. 1). The downward flow induced between the vortices, a so-called down-burst, brings entrained air bubbles into depth. The purpose of this study is to find dominant parameters to determine the distinct types of the

[1] School of Engineering, Hokkaido University, North 13 West 8, Sapporo 060 8628, Japan
[2] City of Sapporo,North 1 West 2, Sapporo 060 8611, Japan
[3] Central Research Institute of Electric Power Industry, 1646 Abiko, Abiko-shi, Chiba 270 1194, Japan
[4] School of Engineering, Hokkaido University, North 13 West 8, Sapporo 060 8628, Japan
[5] School of Engineering, Hokkaido University, North 13 West 8, Sapporo 060 8628, Japan
[6] School of Engineering, Hokkaido University, North 13 West 8, Sapporo 060 8628, Japan
[7] School of Engineering, Hokkaido University, North 13 West 8, Sapporo 060 8628, Japan
[8] School of Engineering, Hokkaido University, North 13 West 8, Sapporo 060 8628, Japan

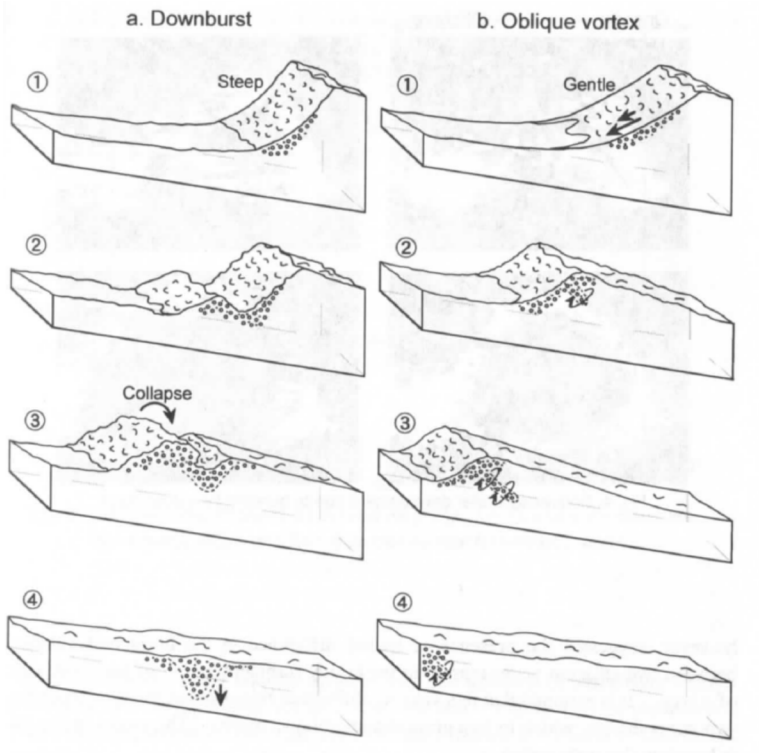

Figure 1. Schematic representations of the downburst (left) and the obliquely descending eddies (right), after Kubo and Sunamura (2001)

surface formation and the flow structure after wave breaking. However, as many mechanical factors affect the surf zone flows, it is difficult to explicitly find a primary parameter to describe the specific local flow in common wave experiments. In order to eliminate many of the factors and to focus only on the effects of the initial plunging jet and water depth to the surface flow dynamics, we perform computational partial dam-break experiments as a simple model of the wave plunging. The surface, vorticity and turbulence responses for splashing and jetting fluid flows, of which the initial conditions are completely controlled by relative collapse height with respective to water depth, are investigated in this paper.

COMPUTATIONAL EXPERIMENTS

In this study, free-surface turbulent flows of a splashing jet have been modeled using an identical model and computational scheme to that described by Watanabe et al. (2009), the approach is summarized in this section as full details are also given in Gotoh, Okayasu and Watanabe (2012).

Computational procedures

The large eddy simulation (LES) approach is used for computing three-dimensional turbulence in this study. In LES, a filtering operation (represented by an overline) is performed on the Navier-Stokes equation and the resulting filtered equation is used as the governing equation:

$$\frac{D_f \overline{\boldsymbol{u}}}{Dt} = -\boldsymbol{\nabla}\overline{p} - \boldsymbol{\nabla}\cdot\boldsymbol{\tau} + \boldsymbol{\nabla}\cdot\overline{\boldsymbol{\tau_0}} + \frac{1}{Fr^2}\boldsymbol{g}', \tag{1}$$

where $\boldsymbol{\tau}$ denotes the sub-grid scale (SGS) stress tensor, $\overline{\boldsymbol{u}}$ is the resolved fluid velocity, $\overline{p}$ is the pressure, $\overline{\boldsymbol{\tau_0}}$ is the viscous stress tensor $(= \frac{2}{Re}\overline{\boldsymbol{S}}$, where $Re\,(= \nu_0/VD)$is the Reynolds number, $\overline{\boldsymbol{S}}$ is the strain tensor and ν_0 is the kinematic viscosity$)$, and $\boldsymbol{g}'$ is the unit gravity vector. $\frac{D_f}{Dt} = \frac{\partial}{\partial t} + \overline{\boldsymbol{u}}\cdot\boldsymbol{\nabla}$

is the filtered material derivative. The second and third terms on the right hand side of Eq. (1) are described by the SGS viscosity equation

$$\boldsymbol{\tau} - \frac{1}{3}(\boldsymbol{\tau} : \boldsymbol{I})\boldsymbol{I} - \overline{\boldsymbol{\tau_0}} = -\frac{2\nu}{Re}\overline{\boldsymbol{S}}, \tag{2}$$

where $\boldsymbol{I}$ is the unit dyadic. The SGS viscosity model based on renormalisation group theory is used to determine ν in Eq. (2).

The location of the free-surface is defined in terms of a level-set function, ϕ, which is defined as a signed distance function from the interface.

$$\frac{D_f\phi}{Dt} = 0. \tag{3}$$

ϕ is taken to be positive inside the fluid and negative outside the fluid. The free surface is defined to be located where $\phi(\boldsymbol{x},\, t) = 0$. Eq.(3) is updated by the Cubic Interpolation Polynomials (CIP) method, which is a quasi-Lagrangian technique for computing advection based on a third-order polynomial interpolation within a cell (see the numerical procedure described by Gotoh, Okayasu and Watanabe (2012)).

Since $\boldsymbol{\nabla}\phi$ is perpendicular to the iso-contour $\phi = 0$, the unit outward normal vector $\boldsymbol{n}$ and the curvature κ of the surface are given by $\boldsymbol{n} = -\frac{\boldsymbol{\nabla}\phi}{|\boldsymbol{\nabla}\phi|}$ and $\kappa = \boldsymbol{\nabla}\cdot\boldsymbol{n}$, respectively. The two unit tangential vectors on the surface are determined by geometric relations with the normal vector $\boldsymbol{n}$. The surface tension and velocity derivatives in the free-surface boundary conditions (4) and (5) can be represented by the level-set function using the above relations.

A jump condition for momentum conservation across a free-surface leads the normal and tangential dynamic boundary conditions on a free-surface:

$$\overline{p_{sf}} + \frac{2\nu}{Re}\frac{\partial\overline{u_n}}{\partial n} = \frac{2\kappa}{We}, \tag{4}$$

$$\frac{\nu}{Re}\left(\frac{\partial\overline{u_n}}{\partial t_i} + \frac{\partial\overline{u_{t_i}}}{\partial n}\right) = 0, \tag{5}$$

where $\overline{p_{sf}}$ is the surface pressure, We ($= \rho V^2 D/\sigma$) is the Weber number, σ is the coefficient of surface tension, and $\overline{u_n}$ and $\overline{u_{t_i}}$ ($i = 1, 2$) are the normal and two tangential components of the resolved surface velocity, respectively.

In the computation of free-surface flows on the fixed grids, where the fluid flow in the air is disregarded, the velocity outside of the fluid region needs to be extrapolated from the inner velocity in order to be able to compute the convective equation and update the surface location. In this study, an extrapolation technique which ensures the zero tangential shear dynamic condition (5) has been used (Watanabe et al. 2008). This approach ensures that in regions of surface deformation with high curvature the correct surface-vortex interactions have been obtained.

A fractional step method has been applied to the discretized form of Eq. (1) — splitting the equation into the convective and non-convective parts. The CIP method is used for the convective step, and then a predictor-corrector method is applied to computing the non-convective equation. A Poisson pressure equation is solved iteratively using a multi-grid method and an irregular-star method is used to prescribed the normal dynamic boundary condition (4) (for details see Gotoh, Okayasu and Watanabe (2012)).

Experimental Setup

LES is performed in a three-dimensional rectangular channel of the domain that is separated by the impermeable wall of height d_w and the lift gate above the wall (See Fig. 2). The water column of depth d_c (= 0.8 m/s) above the wall is collapsed as the gate is lifted at constant velocity of V_0 (= 0.8 m/s), and then the upstream water flows into the ambient water layer of depth d_0. While overflowing splashes are simulated in case $d_w > d_0$, submerged jetting flows occur in case of $d_w <$

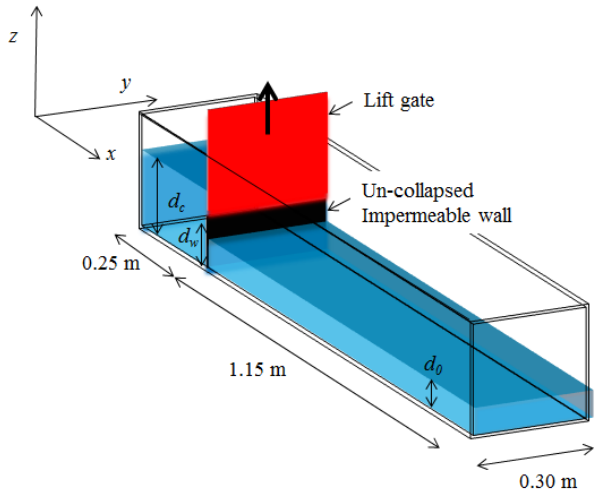

Figure 2. Dam-break tank model.

d_0. Computational grids of 280 in length of the tank, 60 in width, and 58 in height are used to resolve the dimensional domain (1.4 m, 0.3 m, 0.28 m). As periodic flow field is assumed in the spanwise direction, the periodic boundary condition is used on side walls. A non-slip condition is imposed at the bottom boundary. The physical laboratory experiments measuring sequential backlight images of the surface profiles are also performed in the dam-break channel with the same measures to the model domain for validating the computational model.

RESULTS

Distinctive three different modes of the free-surface deformation, vortex formation and the turbulent structure have been found to depend on the relative wall height with respect to forward water layer depth. In $d_w > d_0$, an overflow jet plunges onto a shallower water layer to push the forward water up for projecting a secondary jet forward. In $dw \approx d0$, a rear part of the wave, induced by the initial jetting flow with lower splash angle, forms a planar jet projecting backward owing to surface-vortex interaction; a so-called back-splash is observed. Finally, in $d_w < d_0$, a streamwise array of vortices with the same rotational direction are produced by the submerged jetting flow, and thus vortex-induced blob-like waves are formed there.

Fundamental features for each dam-break mode are discussed bellow.

Plunging Mode

Fig. 3 shows sequences of the experimental and computational surface forms and the coherent vortex structures, visualized by λ_2 method (Jeong and Hussain (1995)), in the case d_w= 10 cm and d_0 = 3 cm. The observed overflow jet plunges with high splash angle (typically $> 45°$) with respect to the surface of the forward shallow water layer at t= 0.18 s. The secondary jet is then ejected forward and overturns to plunge on the surface again (t = 0.25 s and 0.32 s). The computed free-surfaces consistently interpret these major features of the observed surface evolution. We find the transverse array of the coherent vortices stretched from the plunging location to the free edge of the secondary jet (t= 0.25 s in Fig. 3 bottom), forming a rib-like vortex structure (t= 0.32 s) configures identical to the one observed in plunging waves (Watanabe et al. 2005).

The iso-surface of the computed streamwise vorticity at t = 0.32 s is shown in Fig. 4. Multiple pairs of counter-rotating vortices stretched in the axis of the secondary jet are organized in the rib structure. We also find typical spanwise arrangement of scars on the upper surface of the secondary jets before finger jets are formed at the tip of the jet in Fig. 3 (middle), which is caused by the

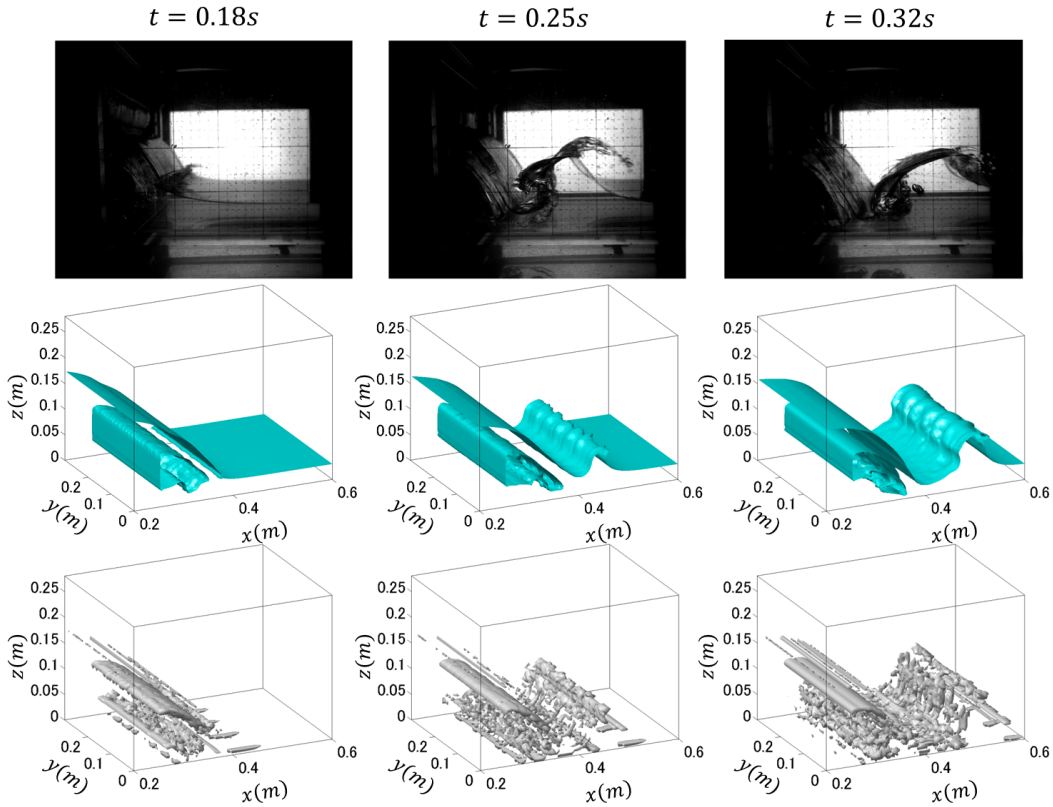

Figure 3. Sequential free-surfaces (top: experimental images, middle: computed results) and coherent vortex structures (bottom) in the case of d_w=10 cm and d_0=3 cm.

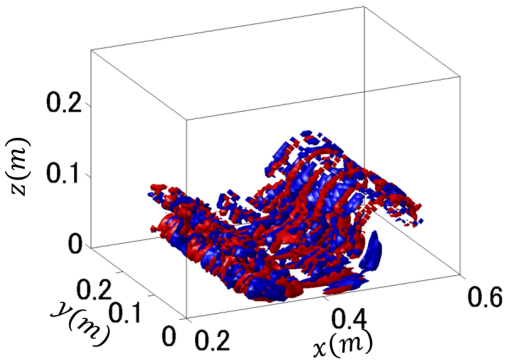

Figure 4. Iso-surface of streamwise vorticity at t = 0.32 s in the case of d_w=10 cm and d_0=3 cm.

entrainment of free-surface by the counter-rotating vortices in the same mechanism interpreted by Saruwatari et al. (2009).

This dam-break mode in $d_w > d_0$, following the overflow with high splash angle, can be an appropriate model for fluid dynamics of wave plunging.

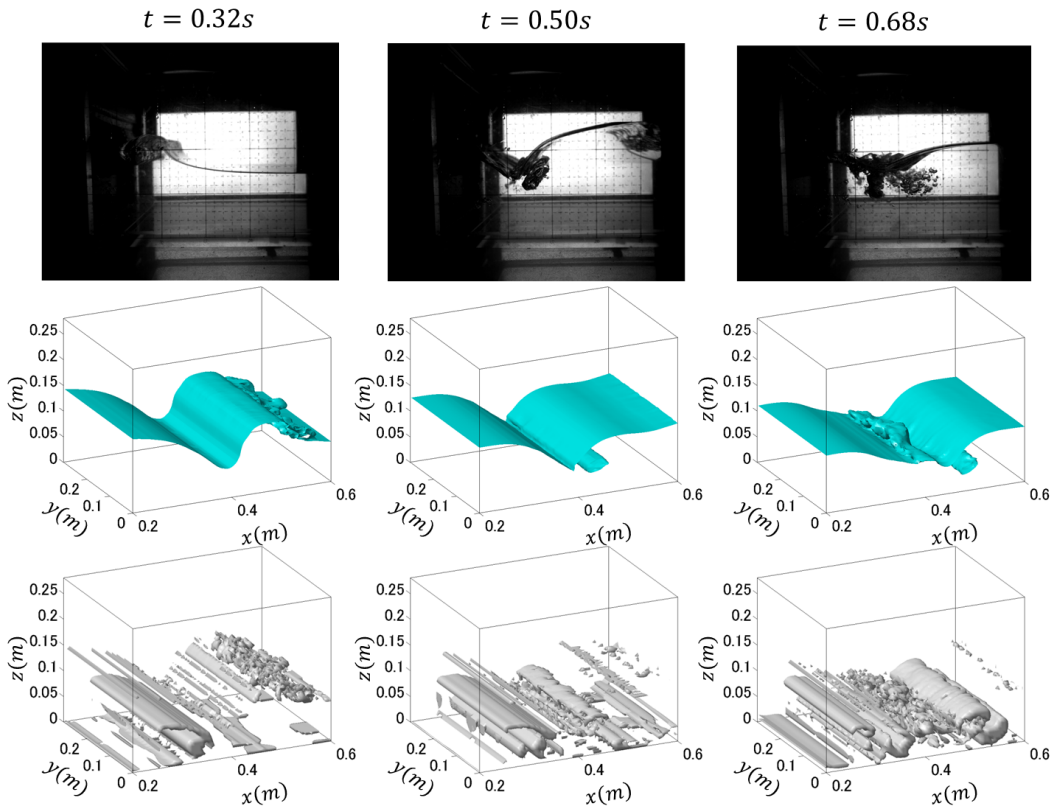

Figure 5. Sequential free-surfaces (top: experimental images, middle: computed results) and coherent vortex structures (bottom) in the case of d_w=7 cm and d_0=7 cm.

Back-Splash Mode

Fig. 5 shows the observed and computed surfaces and the vortex structures in the case d_w= d_0= 7 cm. The initial jetting flow with lower splash angle with respect to the still water surface produces a semi-circular shaped wave with spilling jets at the crest at t=0.32 s. The rear part of the wave projects to the upstream direction and plunges onto the backward wave trough at t=0.50 s before forming the backward secondary jets at t =0.68 s. The emergence of this so-called back-splash is a typical feature of the dam-break flows for $d_w \approx d_0$. A vertically developing bubble plume is observed where the backward jet plunges, in the experimental image at t=0.68 s. In this case, spanwise large-scale horizontal vortices induced by the initial jetting flow govern at t=0.32 s and 0.50 s (see bottom panel of Fig. 5), while an inverse form of the rib structure is organized at the plunging point at t=0.68 s.

Fig. 6 shows the spanwise vorticity on the horizontal vortices at t=0.32 s and 0.50 s. We find a pair of horizontal counter-rotating vortex is simultaneously induced by forward and backward diverging flows from the initial jetting flows. The anticlockwise rotating flow induced by the upper vortex entrains the above surface upstream, resulting in the back-splash; that is, the surface-vortex interaction via the surface entrainment by the sub-surface vortex causes the back-splash event. The analogy of the computed rotating flows, surface form and emergence of the vertical bubble plume with the so-called downburst observed by Kubo and Sunamura (2001) indicates the identical mechanism for the downburst flow with the back-splash dam-break mode. As only parameter of the relative wall height, associated with the orientation of the initial jetting flow, create a difference between the plunging and back-splash modes, we can conclude that the downburst can be

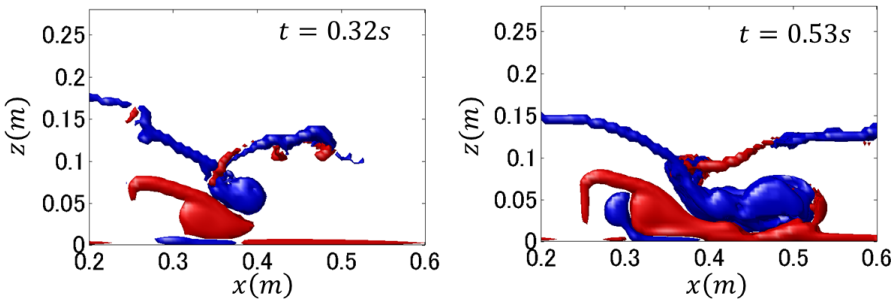

Figure 6. Iso-surface of spanwise vorticity at t = 0.32 s and t = 0.53 s in the case d_w= d_0= 7 cm.

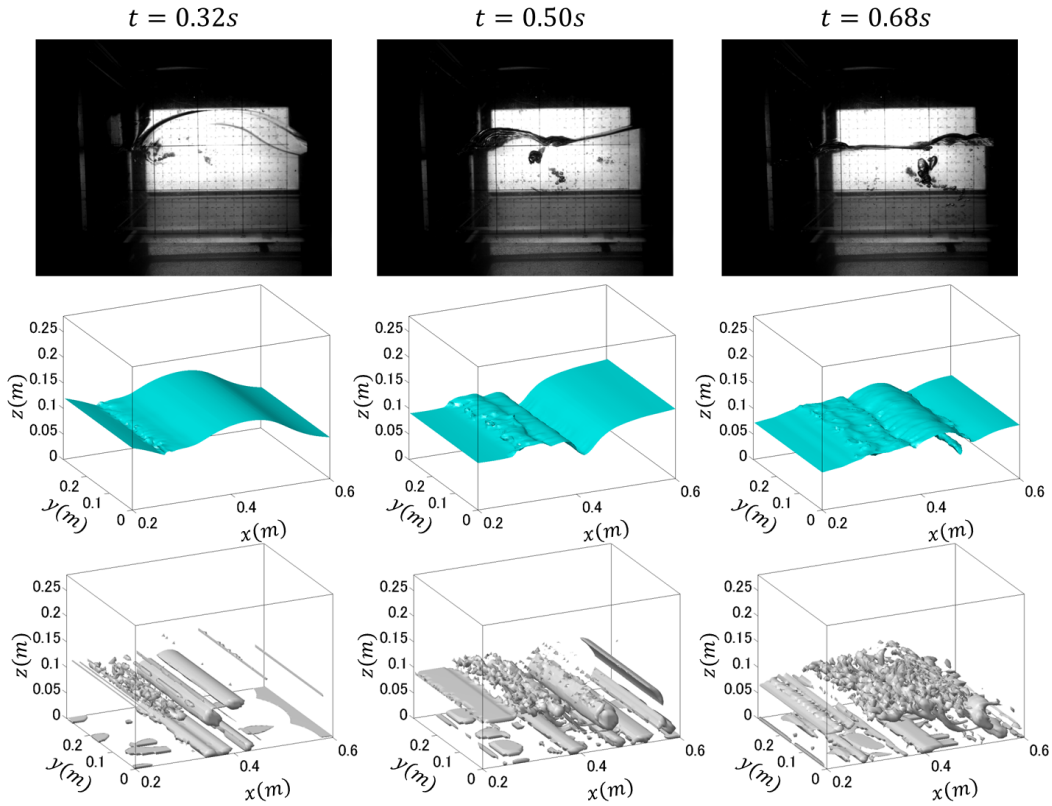

Figure 7. Sequential free-surfaces (top: experimental images, middle: computed results) and coherent vortex structures (bottom) in the case of d_w=0 cm and d_0=7 cm.

parametrized by the splash angle of plunging jet.

Vortex-Induced Wave Mode

In the case $d_w < d_0$, the horizontal jet initially flowing out beneath the submerged gate produce a blob-like wave following multiple horizontal vortices underneath (see t=0.32 s in Fig. 7). As the sub-surface vortices entrain the free-surface above them, a spanwise uniform scar appears at t = 0.5 s and further overturning deformation owing to the vortices is observed to entrap cylindrical air in

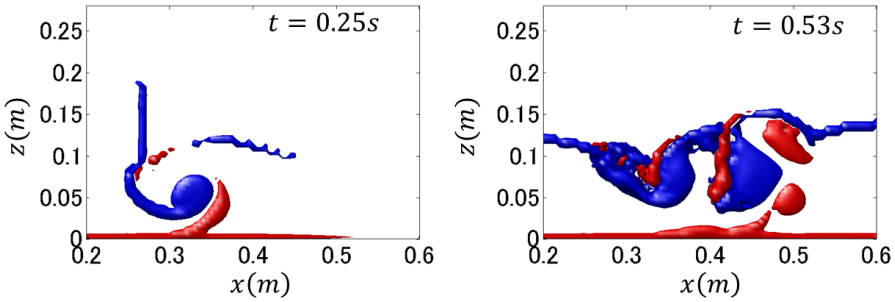

Figure 8. Iso-surface of spanwise vorticity at t = 0.25 s and t = 0.53 s in the case d_w=0 cm and d_0= 7 cm.

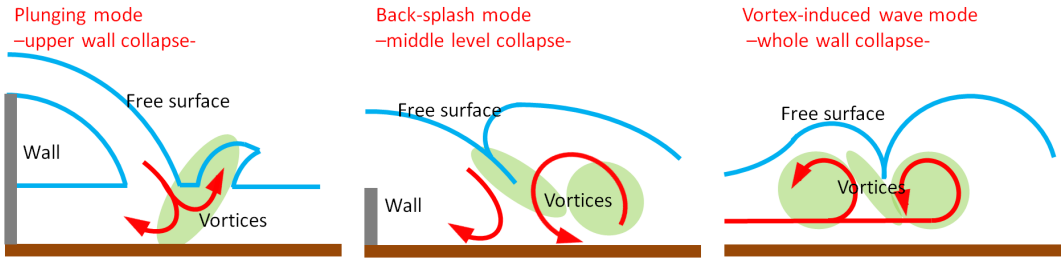

Figure 9. Schematic illustrations of the dam-break flows; plunging mode (left), back-splash mode (middle) and vortex-induced wave mode (right).

the wave at t = 0.68 s. Since strong shear occurs between the horizontal vortices with anticlockwise vorticity (Fig. 8), complex small-scales vortex structure is formed there to disturb the surface above.

These findings on distinct flow patterns depending on the orientation of the plunging jet (or jetting flow) provide new perspectives to understand wave breaking behaviors as well as practical assessments for the fluid responses for overflowing and overtopping.

CONCLUSIONS

In this paper we perform computational partial dam-break experiments as a simple model of the wave plunging to find an primary parameter associated with the surface flows of breaking waves.

Distinctive three different modes of the surface deformation and vortex formation have been found to appear behind the collapsed column, which are summarized in schematic illustrations of Fig. 9.

In $d_w > d_0$, an overflow jet plunges onto a shallower water layer to push the forward water up for projecting a secondary jet forward (Fig. 9 left). The transverse array of longitudinal vortices is stretched from the plunging location to the free edge of the secondary jet, which is identical with the rib vortex structure previously observed in plunging breaking waves (Watanabe et al. 2005).

In $dw \approx d0$, a pair of horizontal counter-rotating vortex is initially produced by jetting flows near the water surface behind the wall (Fig. 9 middle), resulting in a backward splash owing to surface-vortex interaction (surface entrainment by the sub-surface vortex). Since the orientation of the fluid stretch becomes opposite to the previous overflow splash mode, an inverse form of the rib structure is organized in this mode. This counter-rotating fluid motion interprets a fundamental mechanism for producing a so-called downburst observed by Kubo and Sunamura (2001).

In $d_w < d_0$, multiple pairs of counter-rotating vortices are produced by the submerged jetting flow, and thus vortex-induced blob-like waves are formed there(Fig. 9 right).

ACKNOWLEDGMENTS

Financial support for this study is provided by JSPS Grants-in-Aid Scientific Research (243660196, 24360174, 25289150).

REFERENCES

Gotoh, H., A. Okayasu and Y. Watanabe. 2012. *Computational Wave Dynamics*, World Scientific.

Jeong, J. and Hussain, F.. 1995. On the identification of a vortex *J. Fluid Mech.*, 285, 69 – 94.

Kubo H. and T. Sunamura . 2001. Large-scale turbulence to facilitate sediment motion under spilling breakers, *Proc. Coastal Dynamics 2001*, 212 – 221.

Nadaoka, K., M. Hino and Y. Koyano. 1989. Structure of the turbulent flow field under breaking waves in the surf zone *J. Fluid Mech.*, 204, 359 – 387.

Sarpkaya, T. and P. Suthon. 1991. Interaction of a vortex couple with a free surface *Exp. Fluids*, 11, 205 – 2017.

Saruwatari, A. , Y. Watanabe and D. M. Ingram . 2009. Scarifying and fingering surfaces of plunging jets *Coastal Engineering*, 56, 1109 – 1122.

Watanabe Y., H. Saeki and R. J. Hosking . 2005. Three-dimensional vortex structures under breaking waves, *J. Fluid Mech.*, 545, 291 – 328.

Watanabe, Y., A. Saruwatari and D. M. Ingram . 2008. Free-surface flows under impacting droplets, *J. Comp. Phys.*, 227, 2344 – 2365.